ARTICLE

An entorhinal-visual cortical circuit regulates depression-like behaviors

Jian Lu[1,2,3], Zhouzhou Zhang[2,3], Xinxin Yin[2,3], Yingjun Tang[2,3], Runan Ji[2,3], Han Chen[2,3], Yu Guang[4], Xue Gong[1], Yong He[1], Wei Zhou[1], Haiyang Wang[1], Ke Cheng[1], Yue Wang[1], Xiaowei Chen[5], Peng Xie[1]✉ and Zengcai V. Guo[2,3]✉

Major depressive disorder is viewed as a 'circuitopathy'. The hippocampal-entorhinal network plays a pivotal role in regulation of depression, and its main sensory output, the visual cortex, is a promising target for stimulation therapy of depression. However, whether the entorhinal-visual cortical pathway mediates depression and the potential mechanism remains unknown. Here we report a cortical circuit linking entorhinal cortex layer Va neurons to the medial portion of secondary visual cortex (Ent→V2M) that bidirectionally regulates depression-like behaviors in mice. Analyses of brain-wide projections of Ent Va neurons and two-color retrograde tracing indicated that Ent Va→V2M projection neurons represented a unique population of neurons in Ent Va. Immunostaining of c-Fos revealed that activity in Ent Va neurons was decreased in mice under chronic social defeat stress (CSDS). Both chemogenetic inactivation of Ent→V2M projection neurons and optogenetic inactivation of the projection terminals induced social deficiency, anxiety- and despair-related behaviors in healthy mice. Chemogenetic inactivation of Ent→V2M projection neurons also aggravated these depression-like behaviors in CSDS-resilient mice. Optogenetic activation of Ent→V2M projection terminals rapidly ameliorated depression-like phenotypes. Optical recording using fiber photometry indicated that elevated neural activity in Ent→V2M projection terminals promoted antidepressant-like behaviors. Thus, the Ent→V2M circuit plays a crucial role in regulation of depression-like behaviors, and can function as a potential target for treating major depressive disorder.

Molecular Psychiatry; https://doi.org/10.1038/s41380-022-01540-8

INTRODUCTION

Major depressive disorder (MDD) has become a leading cause of disability with more than 264 million sufferers around the world [1]. The prefrontal cortical areas (including dorsolateral, dorsomedial, ventrolateral and ventromedial subareas) have been common targets for stimulation therapy of depression using repetitive transcranial magnetic stimulation (rTMS) or transcranial direct-current stimulation (tDCS) [2–5]. However, the efficacy of therapy is unsatisfactory as it typically requires a chronic treatment course (4 to 10 weeks) [2, 4, 6, 7] and there are high undesirable response rate and remission rate [8–10] (30~50% and 20~40%, respectively). In addition, there are several adverse effects such as headache, skin redness, tinnitus, nervousness and new-onset mania [4, 7]. The visual cortex (Vis) is a novel target for stimulation therapy, and surprisingly, stimulation of Vis can rapidly alleviate depressed symptoms (within 5 days) with little drawbacks [11]. Despite of these desirable properties, how Vis related neural circuits participate in regulation of depression is largely unexplored.

Previous studies have demonstrated that the entorhinal cortex (Ent), a key node that links the hippocampus (HPC) to certain neocortical and subcortical areas, is implicated in depression as characterized by its reduced volume [12], diminished neural activity [13], decreased functional connectivity [14] and abnormal expression of molecules [15–19] in MDD patients or rodent models of depression. Stimulation of Ent and its hippocampal output (from Ent II to DG) can rescue depression-like symptoms and promote learning and memory [20–22]. Enhancing activity of DG newborn neurons or CA1 pyramidal neurons can also promote anxiolytic- and antidepressant-like behaviors [23, 24]. These findings suggest that the hippocampal-entorhinal network is crucial for modulation of depression. The visual cortex, a major output target of this network, receives afferents from Ent layer Va neurons [25–27]. Whether Ent Va output to Vis is implicated in depression and if so, the underlying mechanism remains unknown.

Here, we first used anterograde and retrograde tracers to show that Ent Va neurons had extensive axonal projections to multiple neocortical and subcortical areas and a sub-population of Ent Va neurons mainly targeted the medial part of the secondary visual cortex in the ipsilateral hemisphere (hereafter referred to as Ent→V2M). We then combined c-Fos immunostaining, optogenetic and chemogenetic perturbations, and fiber photometry to delineate the role of the Ent→V2M pathway in depression. Mice under chronic social defeat stress (CSDS) had fewer c-Fos positive neurons in Ent layer Va, indicating that these neurons were less

[1]NHC Key Laboratory of Diagnosis and Treatment on Brain Functional Diseases & Department of Neurology, The First Affiliated Hospital, Chongqing Medical University, 400016 Chongqing, China. [2]IDG/McGovern Institute for Brain Research, School of Medicine, Tsinghua University, 100084 Beijing, China. [3]Tsinghua-Peking Center for Life Sciences, 100084 Beijing, China. [4]Department of gynecology, The First Affiliated Hospital of Shenzhen University (The Second People's Hospital of Shenzhen) and Dapeng Maternity & Child Healthcare Hospital, 518028 Shenzhen, China. [5]Brain Research Center and State Key Laboratory of Trauma, Burns, and Combined Injury, Third Military Medical University, 400038 Chongqing, China. ✉email: xiepeng@cqmu.edu.cn; guozengcai@tsinghua.edu.cn

Received: 20 February 2021 Revised: 28 February 2022 Accepted: 21 March 2022
Published online: 06 April 2022

activated under stress. Mimicking reduced activation, by using chemogenetic inactivation of Ent→V2M projection neurons or using optogenetic inactivation of Ent→V2M projection terminals, recapitulated depression-like behaviors including social deficiency, anxiety, anhedonia and despair-related phenotypes in otherwise healthy mice. Notably, this manipulation also exacerbated depression-like phenotypes in CSDS-resilient mice. Consistently, activation of Ent→V2M projection terminals rapidly rescued behavioral phenotypes of depression, producing an antidepressant effect. Mechanistically, the elevated activity of this pathway promoted the transition from stressed state into anxiolytic- and antidepressant-like state. These findings suggest, for the first time, that the Ent→V2M pathway plays a crucial role in regulation of depression-like behaviors and activity of this circuit drives antidepressant-like behaviors.

METHODS

Animals

Adult male wild type C57BL/6JNju mice (8–10 weeks, from Charles River Laboratories, Beijing) were used for the following experiments: anterograde and retrograde tracing of Ent neurons, chronic social defeat stress and behavior tests, c-Fos immunostaining, chemogenetic and optogenetic manipulations and fiber photometry. Young male C57BL/6JNju mice (4–6 weeks) were used as the stranger mice in three-chamber social test. Adult male Etv1-CreERT2 (Jackson#013048) and *Rosa26*-LSL-H2B-mCherry transgenic mice [28] (8–12 weeks) were used for anterograde tracing of Ent Va neurons' projections at whole-brain level and retrograde tracing of the Ent→V2M projection neurons, respectively. Adult male CD-1 mice (12–16 weeks) were used as aggressors in CSDS. All experimental procedures were approved by the Institutional Animal Care and Use Committee at Tsinghua University, Beijing, China. All mice were maintained in a 12:12 reverse light: dark cycle (light on from 19:00 to next morning 7:00) with water and food *ad libitum*.

Chronic social defeat stress (CSDS)

Similar to the standard protocol [29], CD-1 mice were housed singly and aggressive CD-1 mice were screened primarily. During each day of the 10-day or 21-day CSDS period, each C57BL/6JNju mouse was suffered 5–10 min social defeat stress from an unfamiliar aggressor and then transferred to the other side to experience sensory stress for the remaining day. Control mice were housed in the two sides of the CSDS cage with one mouse per side.

Behavioral experiments

After CSDS, all mice were housed singly with one day interval before behavioral tests. All behavioral tests were similar to previous studies [30–32]. During the test, the mouse was videotaped by a camera from the top to track the movement trajectory or from the side to track the motion. The apparatus was cleaned with a paper towel in 75% ethanol after each session (see supplementary methods for detailed description of apparatus).

Social interaction test (SIT)

Each mouse was introduced into the open area to freely explore for 150 s, after which the mouse was returned to the home cage for an interval of about 30 s. Then the mouse was re-introduced into the open area with an aggressive CD-1 mouse in the enclosure to explore for 150 s. For optogenetic activation experiment, the first part of test with no aggressive CD-1 mouse lasted for 5 min with two 2.5 min periods and laser light was delivered during the second 2.5 min period. The second part of test with a CD-1 mouse lasted for 7.5 min (with pre, optogenetic stimuli, and post periods), and laser were delivered during the second 2.5 min period. The duration that the animal stayed in the interaction zone or corner zones was quantified based on videotaped movement trajectory.

Sucrose preference test (SPT)

Mice were habituated with two bottles of water (one is pure water and the other is 1% sucrose water) for 4 days, with the sides of two bottles switched every day to avoid any side bias. During the one-day test period, the side of the sucrose bottle was randomly set. Consumption of sucrose water or pure water was quantified by measuring the amount of drop of volume in each bottom every day. The sucrose preference = consumption of sucrose water/total consumption of sucrose water and pure water.

For SPT with chemogenetic inactivation of Ent→V2M neurons, mice were water deprived for 12 h to motivate them for water consumption, as the duration of inactivation through applying CNO only lasted for a few hours. During the test, the side of the bottle with 1% sucrose was randomly selected. The test lasted for 2 h.

Elevated-plus maze test (EPM)

Mice were placed into the center and allowed to freely explore the elevated-plus maze for 5.5 min. The durations and entries that animal explored in open arms in the last 5 min were quantified. For optogenetic manipulations, each mouse freely explored in the EPM for 15.5 min, and the laser was delivered from the 5.5 min to 10.5 min.

Forced swimming test (FST)

Mice were individually placed into a glass cylinder (diameter 10 cm, height 30 cm) with water reaching the height of ~20 cm (water temperature ~22 °C) to swim for 6 min. The time that mice spent in immobile (changed area less than 5–7% of their whole-body area) in the last 4 min was quantified. For optogenetic activation, FST lasted for 14 min with laser delivered from the 6th to 10th min. For chemogenetic inactivation, FST lasted for 8 min.

Open field test (OFT)

Mice were individually introduced into the central area of an open field (length, width, height, 46 cm) and allowed to explore for 5.5 min. The duration that animal explored in the central area (length, width, 23 cm), the entries to the central area, and the average speed in the last 5 min were quantified. For optogenetic manipulation, the test lasted for 15.5 min with laser delivered from 5.5 to 10.5 min.

Tail suspension test (TST)

Mice were hung by their tail (~2 cm from the tip, ~30 cm from the ground) using a piece of medical tape. The motion of animal was videotaped from the side for 6 min. The immobile duration in the last 4 min of test was quantified.

Three-chamber social test (TCST)

Three-chamber social test was commonly used to test the sociability of animals [33]. For adaptation, each mouse was introduced into the corridor with the two doors to other chambers closed for 5 min. At the end of adaptation, the doors were opened near simultaneously to allow the mouse freely explore in three chambers for 10 min. To quantify the social interaction, the chambers of S and E were equally divided into two sub-chambers, with S1 and E1 containing perforated cages and the opposite ones, S2 and E2, with no perforated cage. The duration that mice spent in S1, S2, C, E1, E2 was quantified separately. For optogenetic manipulations, laser was delivered during the 10-min test period.

Surgeries and viral injection

Mice were anesthetized by 3–4% isoflurane for 5 min in an acrylic box and then transferred to a surgical table with a stereotaxic apparatus (Kopf Instruments) for head fixation. Mice were placed on a heating pad (~37.5 °C), and ointment (Bepanthen, Bayer) was applied to cover their eyes. The anesthesia was maintained at 1.5–2% isoflurane during the whole surgery period. Flunixin meglumine (Sichuan Dingjian Animal Medicine Co., Ltd) was applied for perioperative analgesia and postoperative pain care (1.25 mg/kg, subcutaneous injection, once a day, at least three consecutive days). A small piece of scalp was removed to expose the skull covering the visual cortex. We performed skull trepanations for manipulation of Ent Va cell bodies or projection-specific manipulations of axon terminals.

For viral injection, mice were unilaterally or bilaterally injected with 150–200 nl of virus at a rate of 50 nl min^{-1} in a brain area by a volumetric injection system (modified from Mo-10 Narishige). The viral vector and injection sites were shown in supplementary methods.

Optogenetic manipulation

For optogenetic activation, 470 nm LED pulse light (NEWDOON Inc., Hangzhou) was delivered at 20 Hz (10 ms on, 40 ms off, square wave) for 500 ms, followed by a 1 s no light interval. The power at fiber tip is about 5 mW. For light blocked experiment, light was delivered as normal but was blocked at the junction of fiber optic cannulae and ferrules. For

optogenetic activation in CSDS mice with blinders, we did behavioral tests of SI, EPM, OFT before and after the animal wearing black blinder, and LED light was delivered as normal. For optogenetic inactivation of the Ent-V2M circuit, orange light from a 594 nm laser (CNI optics, Changchun) was delivered constantly with power (at fiber tip) of 15–20 mW.

Chemogenetic manipulation

The designer drug, Clozapine N-oxide (CNO) (A3317, ApexBio Tech. LLC, USA), was dissolved in DMSO (D8418, Sigma) to form a stock solution of 100 mg/ml which was further diluted to 1.0 mg/ml using 0.9% saline right before use. For SI, TCST, FST and SPT behavioral tests in hM4Di and

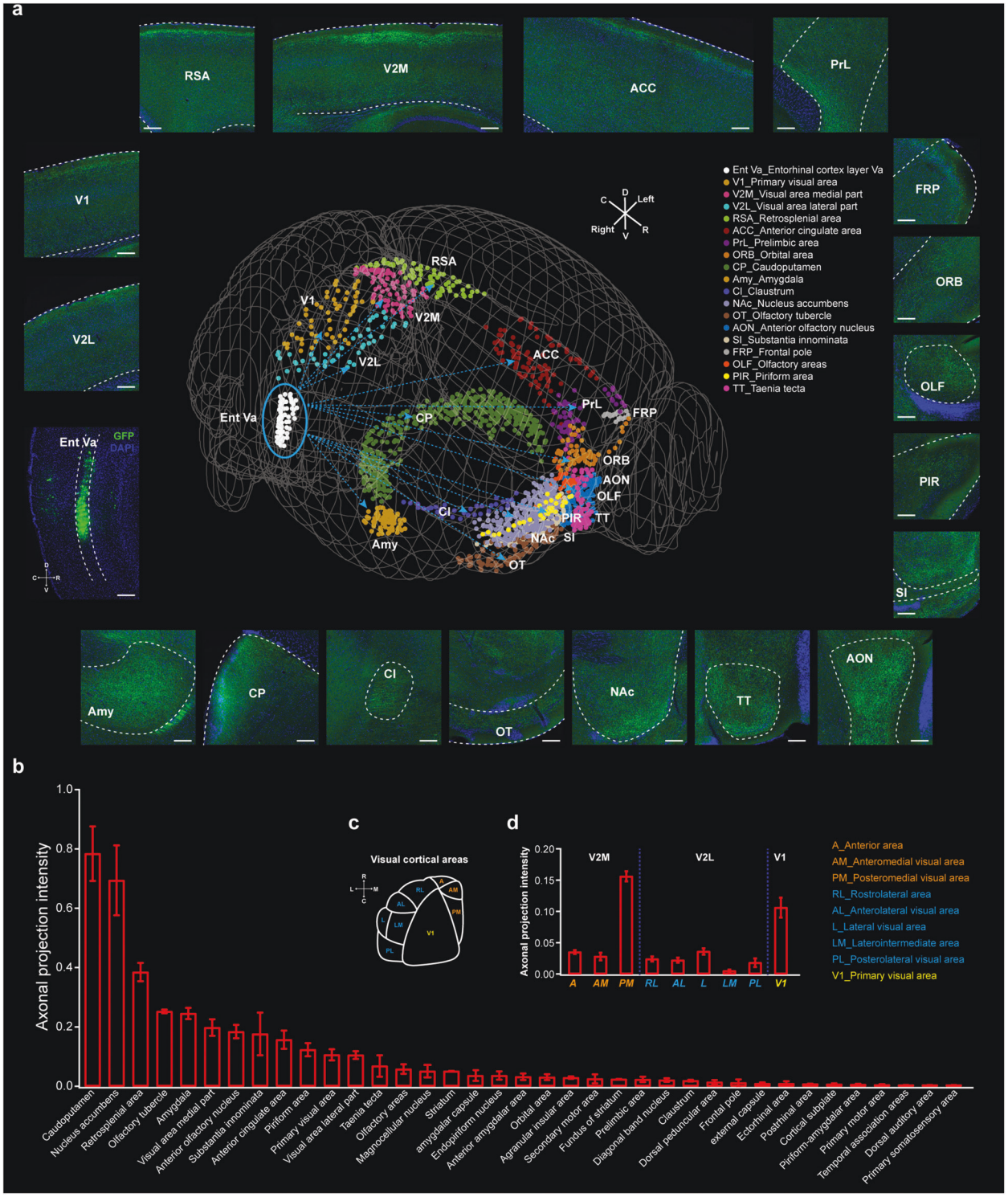

Fig. 1 Brain-wide mapping of Ent Va axonal projections. a Distribution of axonal projections of Ent Va neurons in various cortical and subcortical brain areas. The fluorescence images show example axonal projections. The 3D image (center) indicates the distribution of axonal projections (each dot represents one manually marked sub-region with signals). The locations of these brain regions were shown in Supplementary Fig. 1c. **b** Quantification of axonal projections in 37 cortical and subcortical areas ($n = 3$ mice). **c** Division of the primary and higher-order visual cortical areas. **d** Quantification of axonal projections in the primary and higher-order visual cortical areas ($n = 3$ mice). Scale bars, 200 μm in all fluorescence images.

mCherry mice, CNO was i.p. administrated at 5.0 mg/kg body weight [34, 35] about 50 min before each test. For EPM and OFT, CNO was diluted with 1% sucrose and was administrated intragastrically [36, 37] (i.g., 6–7 mg/kg body weight) using a mouse-feeding needle as this approach potentially reduced disturbance likely seen in i.p. injection.

Fiber photometry

Fiber photometry setup (TINKERTECH, Nanjing) was used to record Ca^{2+} activity under both anesthesia and freely behaving conditions as previous studies [38–40]. To record Ca^{2+} signals of the Ent-V2M circuit, optic fiber with a metal protecting cannula 0.5 mm lower than the fiber tip was implanted onto the surface of V2M. The Ca^{2+} signals and behavioral trajectory during EPM, FST, restraint and reward tests were recoded simultaneously. We used external LED flashes and the corresponding TTL signals to synchronize Ca^{2+} signals and behavioral trajectory (also see supplementary methods).

Immunostaining and imaging of c-Fos

CSDS and control mice were deeply anesthetized one day after behavioral test and were perfused intracardially with PBS followed by 4% PFA. The brains were fixed in 4% PFA overnight and then were dissected to have the hind part containing the whole Ent (left or right). The dissected brains were immunolabelled against c-Fos, and cleared following the recommended iDISCO+ protocol [41]. After clearing, the brains were imaged along lateral to medial axis using a customized light-sheet fluorescence microscope [42] (see supplementary methods for details).

Histology and imaging

Mice were deeply anesthetized by avertin (250 mg/kg bodyweight, T48402, Sigma-Aldrich) and perfused intracardially with PBS followed by 4% PFA. The brains were fixed in 4% PFA overnight and then sectioned into slices (sagittal, 50 μm thickness) by a vibratome (VT1200 S, Leica). Brain sections were imaged by a slide scanner microscope (Zeiss Axio Scan Z1, 10X objective) or confocal microscope (Zeiss LSM710 META, 20X and 40X objectives).

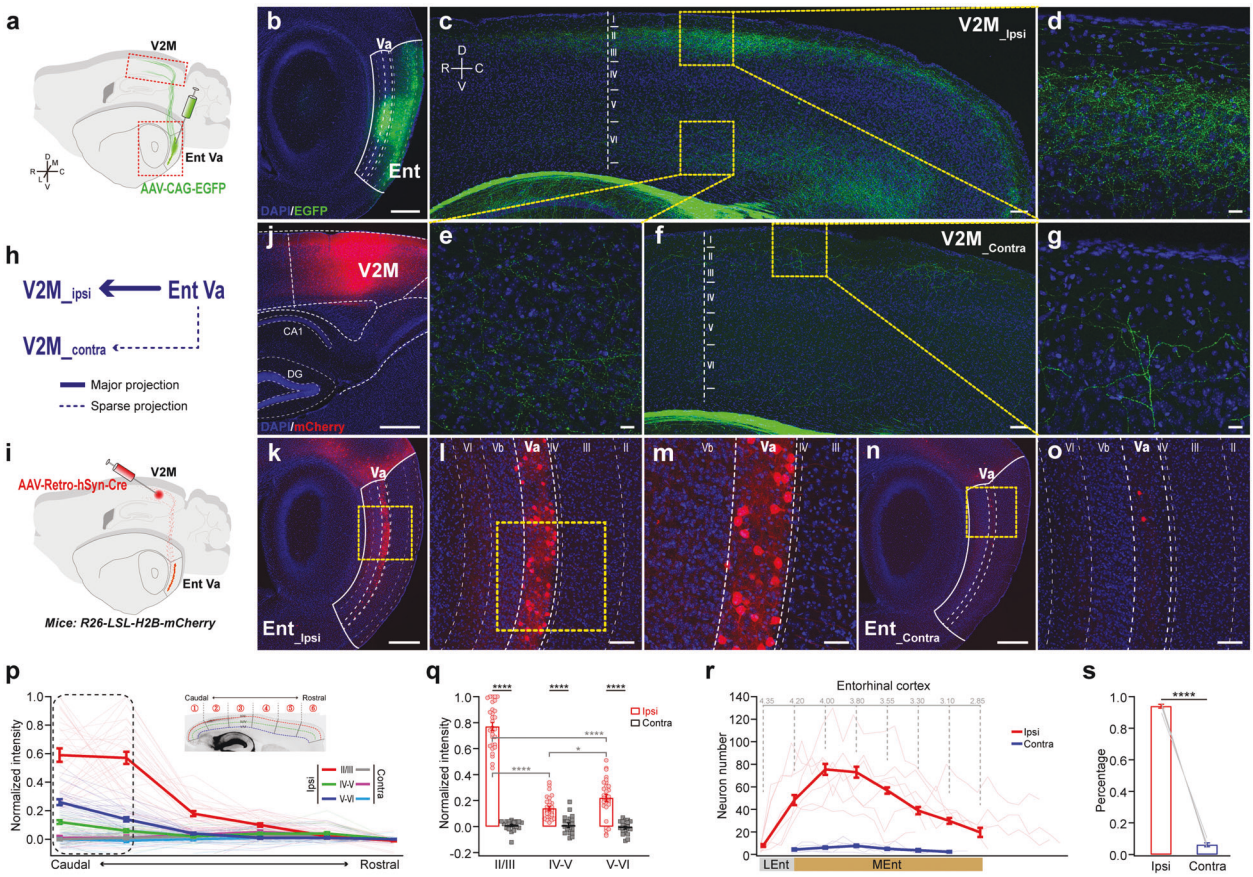

Fig. 2 The entorhinal-visual cortical projections. a Schematic of anterograde tracing of visual cortex projecting Ent Va neurons by injecting AAV-CAG-GFP into Ent Va. Ent, entorhinal cortex; R, rostral; C, caudal; D, dorsal; V, ventral; L, lateral; M, medial. **b** Expression of GFP in Ent with layer Va neurons strongly labeled. Neurons in other layers have little projection to the visual cortex. **c** Distribution of the projections of Ent Va neurons in the ipsilateral medial part of secondary visual cortex ($V2M_{Ipsi}$). **d**, **e** Magnified images of the projections in layers II/III (**d**) and V/VI (**e**) of the visual cortex from **c**. **f** Distribution of the projections of Ent Va neurons in the contralateral V2M ($V2M_{Contra}$). **g** Magnified image of the projections in layer II/III of the visual cortex from **f**. **h** Summary of the Ent→V2M cortical projections. Solid line indicates major projection, dashed line indicates sparse projection. **i** Schematic of retrograde tracing of V2M projected Ent Va neurons by injecting AAV-retro-Cre into the V2M of H2B-mCherry transgenic mice. **j** Expression of mCherry in the injection site in V2M. **k** Distribution of the retrograde labeled Va neurons in the ipsilateral Ent (Ent_{Ipsi}). **l** Magnified view of the boxed region in **k**. **m** Magnified view of the boxed region in **l**. **n** The retrograde labeled Va neurons in the contralateral Ent (Ent_{Contra}). **o** Magnified view of the boxed region in **n**. **p** Density of Ent Va projections from six sections of the ipsilateral or contralateral cortex along caudal-rostral axis (as indicated in the image). Red, green and blue lines indicate the ipsilateral cortical layers of II/III, IV-V and V-VI, respectively. Gray, purple and cyan lines indicate the contralateral cortical layers of II/III, IV-V and V-VI, respectively. The density of the projections was normalized by the strongest cortical projections of each mouse. The density of the ipsilateral or contralateral projection was averaged from over 20 sagittal brain sections collected from at least 3 mice. **q** Quantification of the density of Ent Va projections in different layers of the ipsilateral (red) and contralateral (gray) V2M. Statistics, two-way ANOVA followed by Tukey post hoc test. **r** Quantification of visual cortex-projecting Va neurons in the ipsilateral or contralateral Ent along the lateral-medial axis. Red, ipsilateral Ent ($n = 7$ mice). Blue, contralateral Ent ($n = 5$ mice). **s** Percentage of V2M-projecting Va neurons in the ipsilateral or contralateral Ent. Data were based on the number of neurons from 5 mice. Statistics, paired t-test. Scale bars, 500 μm in **b**, **j**, **k**, **n**; 100 μm in **c**, **f**, **l**, **o**; 50 μm in **m**; 20 μm in **d**, **e**, **g**. $^*P < 0.05$, $^{****}P < 0.0001$. $^*P < 0.05$, $^{****}P < 0.0001$. Data are shown as mean ± s.e.m.

Statistical analysis

Mice were randomly assigned to treatment or control groups. Analyses were performed in a manner blinded to treatment assignments in all behavioral experiments. All statistical analyses were performed using SPSS statistics 20 (IBM). Statistical details including the definitions and exact value of *n* (e.g., number of animals, number of events or trials, etc.), *p* values, and the types of the statistical tests can be found in the Figures and Figure legends (see supplementary methods for details). All statistical tests were two-tailed, and the significance was assigned at $P < 0.05$.

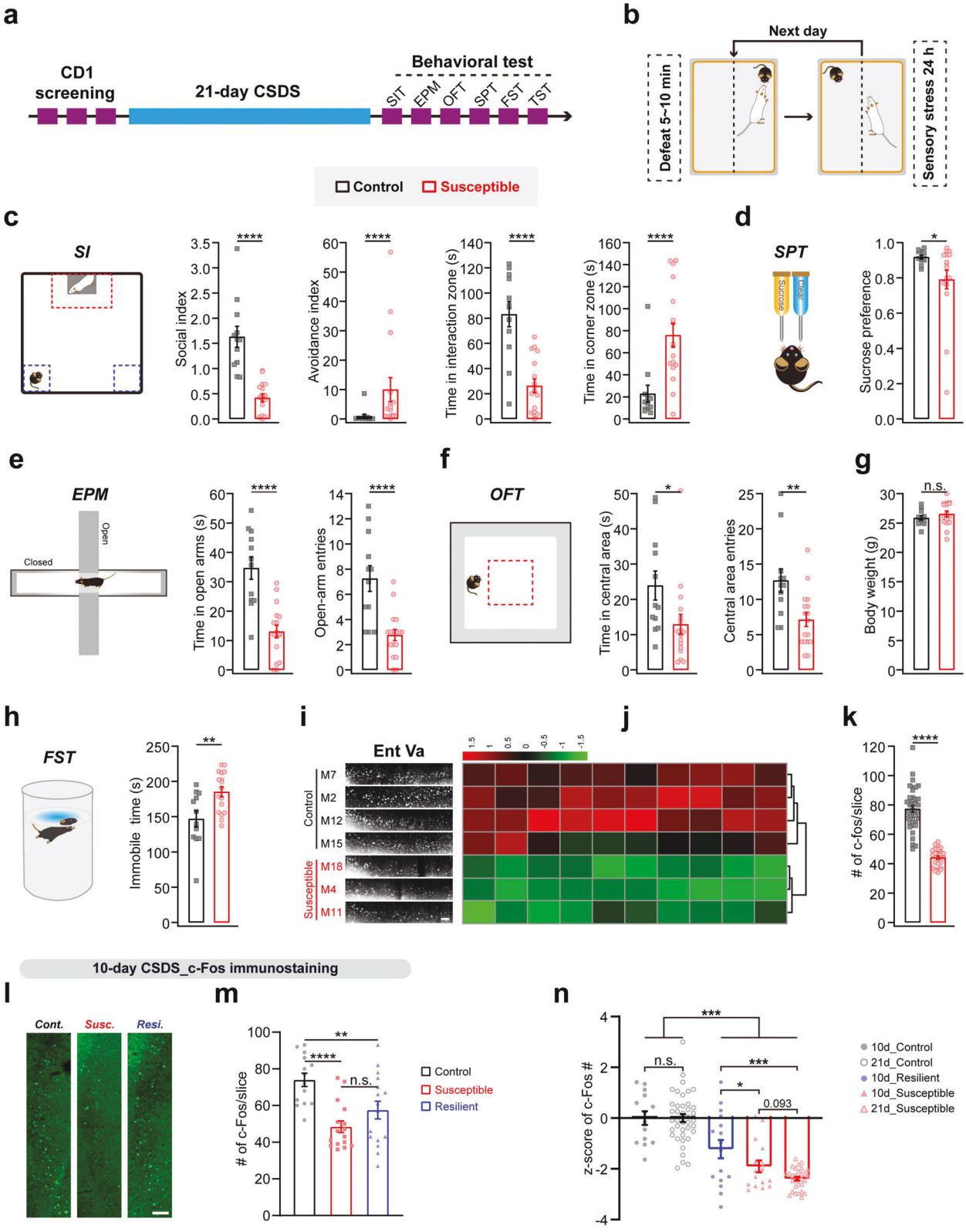

Fig. 3 CSDS decreases the number of c-Fos positive neurons in Ent Va. a Experimental timeline. After 21-day chronic social defeat stress (CSDS), an array of behavioral tests was used to quantify the susceptibility to CSDS. SPT Sucrose preference test, SIT Social interaction test, EPM Elevated-plus maze test, OFT Open field test, FST Forced-swimming test, TST Tail suspension test. **b** Schematic of CSDS. Mice in the CSDS group experienced social defeat stress from a CD-1 mouse for 5–10 min and continuous sensory stress from the same CD-1 mouse during the remaining day. A set of ~25 CD-1 mice were typically used during the CSDS procedure and thus each CD-1 mouse was used once or twice. **c** Schematic of SIT. The social index, avoidance index, times in interaction zone and corner zone were quantified in the control and susceptible mice. **d** Schematic of SPT. Susceptible mice were with significant lower sucrose preference. **e** Schematic of EPM. Susceptible mice had less time and entries in open arms. **f** Schematic of OFT. Susceptible mice showed less time and entries in the central area. **g** There is no significant difference in bodyweight in susceptible and control mice ($P = 0.180$). **h** Schematic of FST. The immobile time in susceptible mice is larger than that in control mice. **i** Example images of c-Fos expression in Ent Va neurons from the control (black labels, $n = 4$) and susceptible (red labels, $n = 3$) mice. **j** Heatmap of c-Fos expression in 10 sections of Ent Va in each mouse from the two groups. **k** Number of c-Fos positive neurons in each section of Ent Va from the two groups. $n = 40$ sections from 4 control mice and 30 sections from 3 susceptible mice. **l** Example images of c-Fos expression in Ent Va neurons of the control, susceptible and resilient mice from 10-day CSDS model. **m** Mean number of c-Fos positive Ent Va neurons of the control, susceptible and resilient mice ($n = 14$ sections from 4 control mice, 16 sections from 4 susceptible mice and 16 sections from 4 resilient mice). **n** Comparison of c-Fos expression among control, susceptible and resilient mice from10-day to 21-day CSDS paradigms. Scale bars, 100 μm in **i** and **l**. Statistics, *t*-test for the behavioral tests. $n = 12$ mice in the control group, 17 mice in susceptible group. Mann-Whitney U test for comparing the number of c-Fos positive neurons between groups and one-way ANOVA followed by LSD post hoc test for comparing z-scored c-Fos expression among different groups from 10-day and 21-day CSDS paradigms. $^{*}P < 0.05$, $^{**}P < 0.01$, $^{***}P < 0.001$, $^{****}P < 0.0001$, n.s. Not significant. Data are shown as mean ± s.e.m.

RESULTS

Brain-wide mapping of axonal projections of Ent Va neurons

Previous studies have shown that Ent Va neurons provide the major output source of Ent to multiple cortical and subcortical areas [25–27]. However, there has not been systematic mapping of Ent Va projections at the whole brain level. To map the brain-wide projections, we first specifically labelled Ent Va neurons using Etv1-CreERT2 transgenic mice (Supplementary Fig. 1). Ent Va neurons labelled with anterograde virus had extensive projections in over 35 cortical and subcortical areas distributed in the neocortex, basal forebrain and striatum (Fig. 1a, b). Among these targets, the caudoputamen and NAc received strongest projections. The Vis, retrosplenial cortex (RSC), anterior cingulate cortex (ACC) and BLA received extensive projections from Ent Va neurons, consistent with previous studies [25–27]. There were multiple brain areas, including olfactory tubercle, substantia innominate and piriform area, that also received extensive projections from Ent Va. For comparison, cortical areas relating to motor, somatosensory and auditory only received sparse projections and there were little projections in the thalamus, hypothalamus, midbrain and cerebellum (Fig. 1a, b and Supplementary Fig. 1c). Within the visual cortex, axonal projections were not uniform, with the anterior, anteromedial and posteromedial regions having highest density of labelling (Fig. 1a, c, d).

Ent Va-visual cortex projection neurons mainly target the ipsilateral V2M

As layer distribution of projection terminals from Ent Va neurons in the neocortex has not been explored, we then combined the anterograde and retrograde strategies to trace the Ent-Vis cortical projections (Fig. 2). Neurons in Ent Va projected extensively to the caudal part of neocortex (mostly in medial part of the secondary visual cortex, V2M) in the ipsilateral hemisphere with relatively little projections in the contralateral hemisphere (Fig. 2a–g, Supplementary Fig. 2). Notably, axons from Ent Va neurons mainly targeted the supragranular layers (II/III) rather than infragranular layers (IV-VI) of V2M (Fig. 2p, q and Supplementary Fig. 2g–i).

To further confirm that Ent Va neurons project to V2M, we injected retrograde recombinant adeno-associated virus (rAAV2-retro-hSyn-Cre) into V2M of *Rosa26*-LSL-H2B-mCherry transgenic mice (Fig. 2i, j). V2M projecting neurons were mainly located in layer Va of the ipsilateral Ent (Fig. 2k–o and Supplementary Fig. 3). As Ent Va neurons project to Vis, PFC, NAc and BLA, we check whether V2M projecting Ent Va neurons represent a distinct population. To do so, we did dual retrograde virus injection with rAAV2-retro-hSyn-tdTomato injected into V2M and rAAV2-retro-hSyn-GFP injected into PFC, NAc, or BLA. Few Ent Va neurons (less than 10%) showed co-labeling of tdTomato and GFP, indicating that V2M projecting Ent Va neurons were largely distinct from those projecting to PFC, NAc or BLA (Supplementary Fig. 4). Moreover, we found that V2M projecting Ent Va neurons were mainly in the medial part of Ent (MEnt) (Fig. 2r, s). Thus, a subpopulation of Ent Va neurons preferentially targeted the supragranular layers of the ipsilateral V2M (Fig. 2h).

CSDS decreases activity in Ent Va neurons of both susceptible and resilient mice

As the 21-day CSDS paradigm can induce higher uniformity in depression-like behaviors [30], we first applied this paradigm to efficiently induce depressed mice (Fig. 3a, b). After 21 days of CSDS (Fig. 3b), most of mice reliably exhibited depression-like behaviors (hereafter referred to as susceptible mice) (Fig. 3c–h). Compared with control mice without going through the CSDS procedure, susceptible mice had significantly reduced social interaction (Fig. 3c) and sucrose preference (indicating anhedonia, Fig. 3d), increased level of anxiety in elevated-plus maze (EPM) and open field (OFT) tests (Fig. 3e, f), and increased immobile time in the forced-swimming test (indicating despair, Fig. 3h). Compared with control mice, susceptible mice showed no significant difference in body weight (Fig. 3g) and immobile time in tail suspension test (TST) (control group vs. susceptible group is 160.4 ± 11.4 s vs. 176.5 ± 9.6 s). The locomotion speed of susceptible mice is slight but significantly lower than that of control mice (Supplementary Fig. 5a). However, there was no significant correlation between time spent in central area and locomotion speed (Supplementary Fig. 5b). These results suggest that the CSDS paradigm can robustly induce depression-like behaviors in mice.

To test whether CSDS changed neural activity in Ent Va neurons, we immunostained c-Fos (a marker for neuronal activation, Supplementary Fig. 5c). Susceptible mice had less activated neurons compared with control mice, as characterized by reduced number of c-Fos positive neurons in Ent Va (Fig. 3i). This pattern of reduction was consistent across consecutive slices and the number of c-Fos positive neurons in each section was significantly smaller in susceptible mice (Fig. 3j, k).

To test whether activity in Ent Va neurons was also reduced in resilient mice, we adopted the standard 10-day CSDS paradigm [29] in order to have more resilient mice (Supplementary Fig. 6). Compared with susceptible mice, resilient mice showed significant more social interaction and higher sucrose preference (Supplementary Fig. 6c–g). Resilient mice showed no difference in FST, EPM and OFT tests (Supplementary Fig. 6h–l). We then checked the number of c-Fos positive Ent Va neurons in resilient mice

(Fig. 3l–n). Resilient mice had significant reduced number of c-Fos positive neurons than control mice although the reduction was less compared with susceptible mice (Fig. 3l–n). The variable reduction level in susceptible mice provided an opportunity to study the relation between Ent Va activation and depression. The number of c-Fos positive neurons in Ent Va was positively correlated with the social index, time in interaction zone, sucrose preference, time in central area and central area entries in OFT, and negatively correlated with immobile time in FST (Supplementary Fig. 5d–i). These results demonstrate that CSDS reduces neural activity in Ent Va neurons of both susceptible and resilient mice and suggest that the number of activated Ent Va neurons predicts the susceptibility of depression.

Inactivation of Ent→V2M projection neurons in healthy mice recapitulates depression-like behaviors

To test whether the Ent→V2M pathway is causally involved in regulating depression-like behaviors, we injected cre-dependent hM4Di virus (AAV9-EF1a-DIO-hM4Di-mCherry, Gi-DREADD [43]) in Ent Va and injected retrograde Cre virus (AAV2-retro-hSyn-Cre) in V2M, to specially label V2M projecting Ent Va neurons (Fig. 4a). We inactivated Ent Va neurons in wild type mice to mimic the reduced activity in CSDS susceptible mice. Inactivation of Ent→V2M projection neurons following injection of CNO (5 mg/kg body weight [34, 35]) was verified by monitoring calcium-evoked neural activity using fiber photometry (Fig. 4b–d).

Inactivation produced depression-like phenotypes in multiple tests (Fig. 4e–m). In the three-chamber social test (TCST), hM4Di mice was not attracted to interact with a stranger mouse at location S1, but rather spent more time with a perforated columniform cage placed at E1, resulting in a reduced social preference (defined as time spent at S1 divided by time spent at E1, Fig. 4e, f). Furthermore, hM4Di mice exhibited significant higher level of anhedonia, despair, and anxiety compared with mCherry control mice, as indicated by decreased sucrose preference (Fig. 4h), longer immobile time in FST (Fig. 4j), less central area duration and entries in OFT (Fig. 4k) and less open-arm duration and entries in EPM (Fig. 4l). In contrast, hM4Di mice injected with saline showed no difference in sucrose preference (Fig. 4i) and time and entries to open arms of EPM (Fig. 4m). The speed of locomotion in hM4Di mice was not significantly different in TCST but was reduced in OFT (Supplementary Fig. 7a, d). However, there was no significant correlation of time spent in S1, E1 or central area with movement speed (Supplementary Fig. 7b, c, e), suggesting that the altered level of sociability and anxiety cannot be explained by reduced locomotion speed. Furthermore, the time in corridor of TCST and the immobile time in the first 2 min of FST showed no significant difference, confirming that inactivation did not affect the locomotion capability (Fig. 4g, j). Taken together, inactivation of Ent→V2M projection neurons in wild type mice recapitulates depression-like behaviors, suggesting that the Ent→V2M pathway is causally involved in regulation of depression.

Ent→V2M projection neurons represent a distinct population in layer Va from those projecting to PFC, NAc or BLA (Supplementary Fig. 4), suggesting that our results were not due to inactivation of collateral projections to other brain areas. To further confirm this, we optogenetically suppressed neural activity of Ent Va projection terminals in V2M (Supplementary Fig. 8). We first injected virus into Ent bilaterally to allow expression of ArchT in Ent Va neurons and their axonal projections in V2M (Supplementary Fig. 8c, d). During behavioral test, we delivered light through optical fibers implanted over V2M to bilaterally illuminate Ent projection terminals (constant light, 15–20 mW/side as inactivation of axons requiring higher power, Supplementary Fig. 8e, f). ArchT mice exhibited higher anxiety in EPM with reduced exploration time in open arms compared with GFP control mice (Supplementary Fig. 8g). ArchT mice also interacted less with stranger mice in TCST (Supplementary Fig. 8h, i), indicating deficit in sociability under inhibition of Ent→V2M pathway. These results further confirm that the V2M projecting Ent Va neurons regulate depression-like phenotypes through their direct projections.

Inactivation of Ent→V2M projection neurons aggravates depression-like phenotypes in resilient mice

As resilient mice showed no obvious change in social interaction and sucrose preference tests compared with control (Supplementary Fig. 6), we wonder whether inactivation of the Ent→V2M pathway can still induce depression-like behaviors. To check this, we performed the same chemogenetic inactivation but in resilient mice (Fig. 5a). Following inactivation, resilient mice exhibited significant higher level of social avoidance and anxiety compared with the same set of mice before inactivation, as indicated by decreased social index and time in interaction zone (Fig. 5b, c), less open-arm duration and entries in EPM (Fig. 5h, i), and less central area duration and entries in OFT (Fig. 5j, k). Resilient mice also showed higher time in corner zone, higher avoidance index in SIT, higher immobile time in FST and lower preference for sucrose, although the change was not significant (Fig. 5d–g). Notably, these resilient mice did not exhibit difference in social avoidance, sucrose preference and anxiety before inactivation. Thus, suppressing activity of Ent Va→V2M projection neurons also aggravated the depression-like phenotypes in resilient mice.

Activation of Ent→V2M projection terminals rapidly alleviates depression-like phenotypes

Given that the Ent→V2M pathway causally contributes to depression-like behaviors, we hypothesized that activating this pathway could rescue behavioral symptoms of depression. To test this, we virally injected the excitatory opsin ChR2 (AAV2/9-CaMKIIa-hChR2(H134R)-EYFP) in Ent of CSDS mice (Fig. 6a, e, i). As only Ent Va neurons project to V2M, we took advantage of this feature to specifically activate the Ent→V2M pathway by optically stimulating axonal terminals in V2M (Fig. 6f). Stimulation of projection terminals (470 nm LED, 5~6 mW) reliably induced postsynaptic Ca^{2+} activities in V2M (Fig. 6b), with evoked activity having an amplitude similar to spontaneous activity (Fig. 6c, d).

We next assessed the behavioral effects during bilateral activation of the Ent→V2M pathway (Fig. 6g–i). Stimulation alleviated depression-like phenotypes in multiple tests. In SIT, the abnormality in social index and avoidance index disappeared during optogenetic activation of the Ent→V2M pathway (Fig. 6j, k). The abnormality also disappeared in a variety of behavioral tests including EPM (Fig. 6n, o), OFT (Fig. 6p, q), FST (Fig. 6r) and TST (Fig. 6s). Specifically, susceptible mice showed significantly increased time in social interaction zone (Fig. 6l, m), in open arms in EPM (Fig. 6n) and in central area in OFT (Fig. 6p), and exhibited increased entries to open arms of EPM and to central area of OFT (Fig. 6o, q) during optogenetic stimulation. The time in corner zone of SIT and the immobile time in FST and TST tests were significantly reduced (Fig. 6m, r, s). The difference between time in interaction zone and time in corner zone of SIT was also diminished (Fig. 6m). Activating the Ent→V2M pathway can promote animals to be more active as indicated by significantly increased locomotion speed of both groups in OFT (Supplementary Fig. 8j). However, there were no correlation between duration in central area and locomotion speed under control and optogenetic activation conditions (Supplementary Fig. 8k, l). Control mice (injected with ChR2 but without CSDS) also exhibited improvement in most of tests (EPM, OFT, FST, and TST), suggesting that elevating neural activity of the Ent→V2M pathway can generally ameliorate depression-like phenotypes (Fig. 6n–s). To further confirm this, we activated this pathway in a new cohort of wild type mice (Supplementary Fig. 8g–i). The sociability of healthy mice was notably improved in TCST as indicated by significantly increased social interaction duration in S1 and

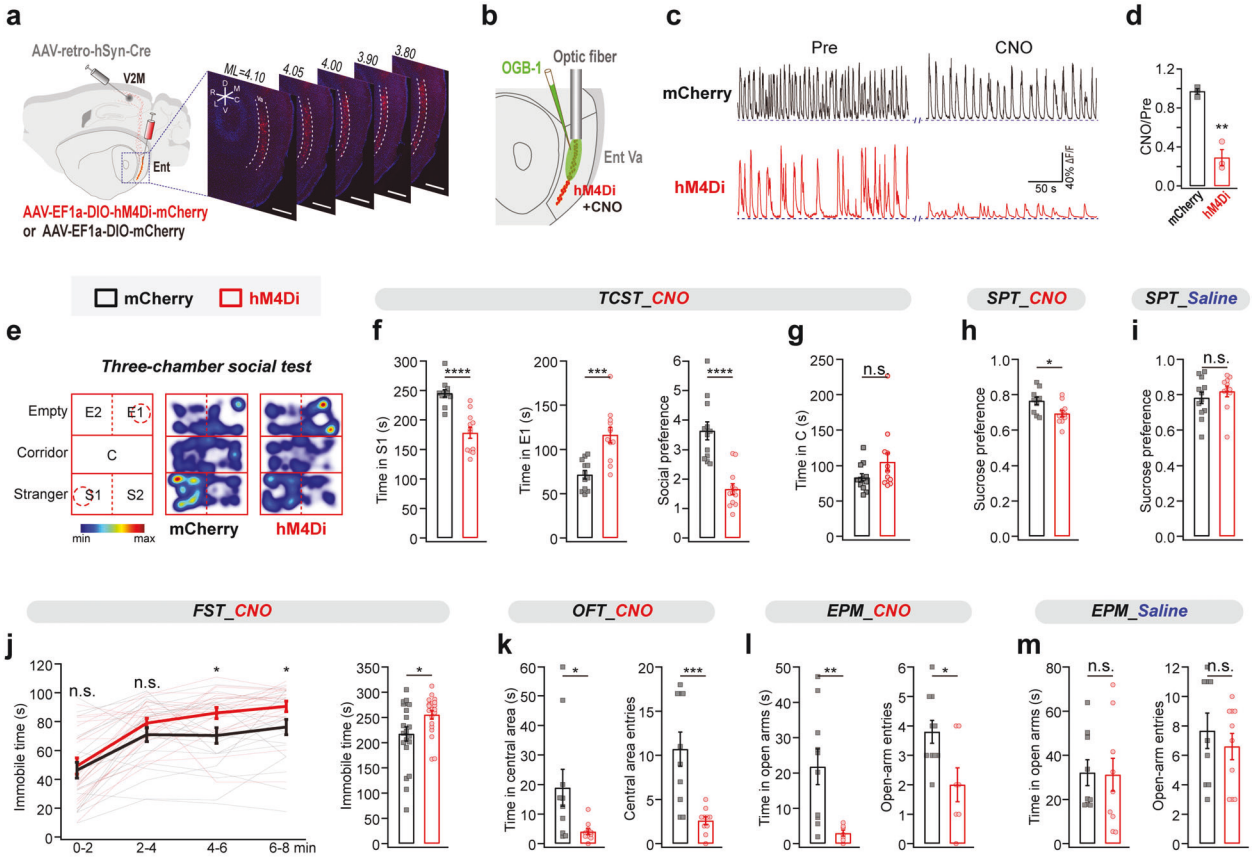

Fig. 4 Inactivation of Ent→V2M projection neurons induces depression-like behaviors. a Schematic of specifically labelling of V2M projecting Ent Va neurons using cre-dependent hM4Di and retrograde cre. To label Ent→V2M projection neurons specifically, we virally injected AAV-retro-hSyn-cre into V2M and injected AAV-EF1a-DIO-hM4D(Gi)-mCherry (hM4Di group) or AAV-EF1a-DIO-mCherry (Control group) into Ent Va bilaterally. This dual viral injection strategy yielded specific labeling of Ent Va neurons. R, rostral; C, caudal; D, dorsal; V, ventral; L, lateral; M, medial. Scale bars, 500 μm. **b** Schematic of functional test of hM4Di using fiber photometry in vivo. Ca^{2+} fluorescent dye (OGB-1, AM) was injected into Ent Va and an optical fiber was implanted there to record neural activity before and after intraperitoneal injection of CNO. **c** Example fluorescent traces in hM4Di (red) and mCherry (black) mice before and after CNO injection. **d** The normalized amplitude of fluorescence fluctuations (CNO/Pre) in hM4Di mice is significantly smaller than that in control mice ($n = 3$ for both hM4Di mice and mCherry mice). **e** Schematic of the three-chamber social test (left) and example trajectory heatmap in mCherry mice (middle) and hM4Di mice (right). The hM4Di mouse spent less time in S1 interacting with a stranger mouse. **f** Quantification of social interaction of hM4Di mice. With bilateral inactivation of V2M projecting Ent Va neurons, hM4Di mice spent less time interacting with stranger mice (left) but spent relatively more time in E1 (without stranger mice, middle) compared with mCherry control mice. The social preference, defined as time in S1 over time in E1, is much lower for hM4Di mice compared with control mice (right). $n = 12$ for both hM4Di and mCherry mice. **g** The time that mice explored in corridor from both groups shows no significant difference ($P = 0.126$). **h, i** hM4Di mice had lower sucrose preference than that of mCherry mice after injection of CNO (**h**). The two groups showed no difference after injection of saline without CNO (**i**). $n = 10$ hM4Di mice and 11 mCherry mice in **h**; $n = 12$ hM4Di mice and 11 mCherry mice in **i**. **j** In FST, hM4Di mice spent more time immobile than mCherry mice. The immobile time in each two-minute duration (left) and in the last 6 min (right) were compared between hM4Di mice ($n = 20$) and mCherry mice ($n = 21$). **k** hM4Di mice explored less (duration and entries) in central area in OFT. $n = 10$ hM4Di mice and 10 mCherry mice. **l, m** In EPM, the duration in open arms and entries to open arms are significantly less for hM4Di mice compared with mCherry mice (**l**). The two groups of mice showed no difference in duration and entries (**m**) without CNO. $n = 7$~10 mice in each group. Statistics, two-way ANOVA with Bonferroni post hoc test in **j** and *t*-test for other behavioral results. $^*P < 0.05$, $^{**}P < 0.01$, $^{***}P < 0.001$, $^{****}P < 0.0001$, n.s. Not significant. Data are shown as mean ± s.e.m.

decreased duration in E1 relative to GFP mice (Supplementary Fig. 8h). Consistently, these mice also exhibited a lower level of anxiety as indicated by the longer exploration time in open arms in EPM (Supplementary Fig. 8g). These results suggest that activation of the Ent→V2M pathway rapidly alleviates depression-like phenotypes and this pathway could bidirectionally regulates depression-like phenotypes both in healthy and CSDS mice (Figs. 4–6, Supplementary Fig. 8).

Activity of the Ent→V2M projection terminals promotes antidepression

To investigate how the Ent→V2M pathway mediates depression-like behaviors, we virally expressed genetically encoded Ca^{2+} indicators (jGCaMP7b [44]) in Ent Va and used fiber photometry to monitor neural dynamics of their terminals in V2M (Fig. 7a, b, Supplementary Fig. 9a–c). Fluorescent signals showed spontaneous fluctuations under both anesthesia and freely moving conditions in jGCaMP7b mice, but not in control EYFP mice, indicating that fluorescence change reflected activity of the Ent→V2M pathway (Supplementary Fig. 9d–f).

We next monitored neural activity of the Ent→V2M projection terminals during several behavioral tests. In EPM, activity was significantly higher when mice were in the center and open arms than in closed arms (Fig. 7c–e). When mice crossed from the closed arms to open arms (approach), neural activity increased typically seconds before the beginning of transition (Fig. 7c, f). In contrast, the activity decreased when mice moved from open to closed arms (retreat) (Fig. 7f, g). Furthermore, activity responded

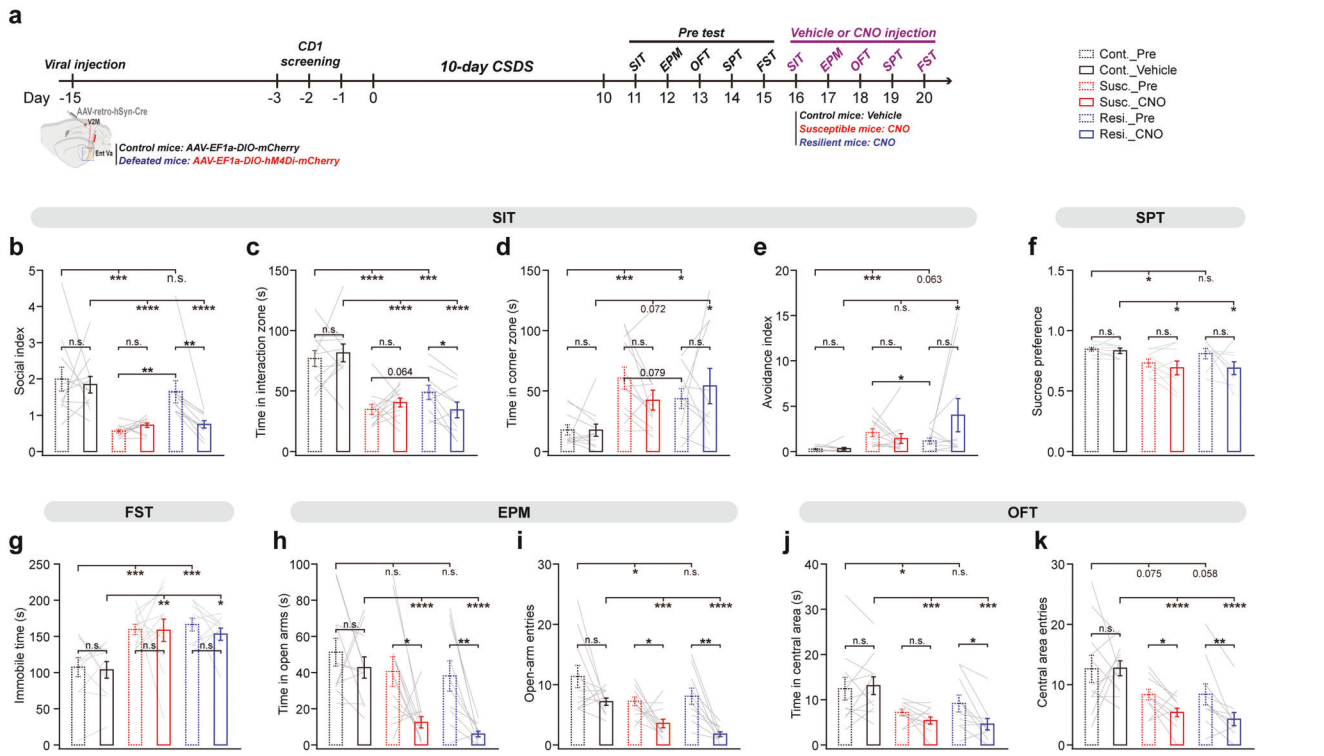

Fig. 5 Inactivation of Ent→V2M projection neurons promotes depression-like behaviors in resilient mice. a Experimental timeline of viral injection, 10-day CSDS, behavioral test without or with chemogenetic inactivation. **b**–**e** The social index, times in interaction zone and corner zone, and avoidance index were quantified among control, susceptible and resilient mice before and after injection of CNO or saline. **f** The sucrose preference of control, susceptible and resilient mice. Susceptible and resilient mice after CNO injection showed significantly reduced sucrose preference compared with control mice. **g** Susceptible and resilient mice showed longer immobile time compared with control mice. **h**, **i** Resilient mice showed significant less time in and entries to open arms after CNO injection. **j**, **k** Resilient mice showed significant less time in and entries to central area after CNO injection. Statistics, two-way ANOVA followed by LSD post hoc test for intragroup comparison. $^{****}P < 0.0001$, $^{***}P < 0.001$, $^{**}P < 0.01$, $^{*}P < 0.05$, n.s. not significant. $n = 11$ mice in the control group, 12 mice in the susceptible group and 10 mice in the resilient group. Data are shown as mean ± s.e.m.

continuously to milk reward (Fig. 7h–j). The increase of amplitude during the reward phase did not correlate with licking duration (the number of licks), suggesting that activity of the pathway did not reflect licking movement itself (Fig. 7k). During FST, the activity of the Ent→V2M projection terminals correlated with the anti-despair state (indicated by the mobile state) (Fig. 7l), and the rise of activity was ahead of the transition from immobile state to mobile state (Fig. 7n). In the restraint test, the activity of the Ent→V2M pathway also correlated with the anti-restraint state and activity increased nearly 1 s before the transition from the quiet to resistant state (Fig. 7m, o). This activity increase is unlikely due to movement itself since the Ent→V2M pathway did not respond to simple motion such as continuously running on a treadmill or grooming (Supplementary Fig. 10). Directly activating the Ent→V2M pathway rapidly alleviates depression-like behaviors (Fig. 6). Thus, activity increase of the Ent→V2M pathway drives antidepression and can potentially function as an antidepressant.

The antidepressant effect does not depend on external visual input

As visual stimulus can modulate mood and depression through the retina to subcortical areas including LHb, NAc and superior colliculus (SC) [45–47], we have used multiple approaches to control that the antidepressant effect of activating the Ent→V2M projection terminals is independent of external visual input. We first ruled out the possibility that leaked light contributed to the antidepressant effect (Supplementary Fig. 11a). With optogenetic stimulation blocked but leaked light unchanged, susceptible mice showed no improvement in sociability and the anxiety level was not changed (Supplementary Fig. 11b–i). We then blocked visual stimulus due to leaked light by covering eyes of mice with blinders (Supplementary Fig. 11j). With eyes covered, susceptible mice showed no significant change in sociability and anxiety (Supplementary Fig. 11k–n), indicating that blocking normal vision did not alter basic behaviors. However, with activation of the Ent→V2M pathway, susceptible mice with blinders still showed reduced depression-like phenotypes in SIT, EPM and OFT tests (Supplementary Fig. 11k–n). These results demonstrate that the antidepressant effect during activation of the Ent→V2M pathway is independent of the peripheral visual pathway.

Given that the Ent→V2M pathway regulates depression-like behaviors independent of the peripheral visual input, we hypothesize that diminishing visual inputs or presenting additional visual stimuli would not alter neural dynamics of the Ent→V2M projection terminals. To test this, we first monitored activity of the Ent→V2M pathway under both white-light and red-light conditions in EPM and restraint tests (Fig. 7a–g, m, o, Supplementary Fig. 12a, d). Neural activity under red-light condition is not significantly different from that under white-light condition in EPM and restraint tests (Supplementary Fig. 12b, c, e, f). Next, we delivered ten consecutive blue light flashes and simultaneously recorded neural activity of the pathway using fiber photometry (Supplementary Fig. 12g). Consecutive visual flashes, especially late flashes, did not effectively activate the Ent→V2M pathway (Supplementary Fig. 12h–j). These results suggest that the Ent→V2M circuit modulates depression-like behaviors independent of the peripheral visual input.

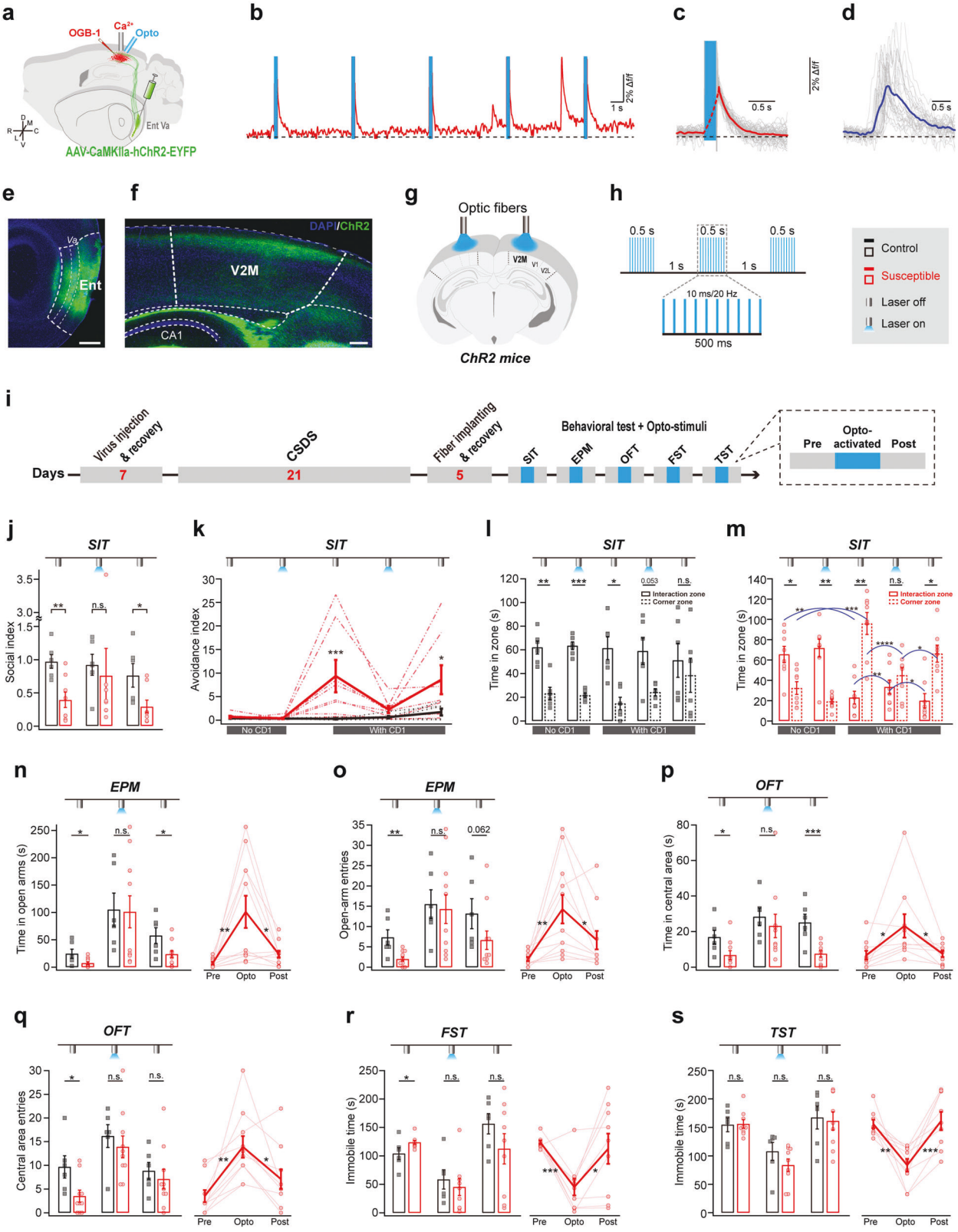

DISCUSSION

Our study provides the first evidence to our knowledge that the Ent→V2M pathway can bidirectionally regulates depression-like behaviors. Specific inactivation of the Ent→V2M pathway in healthy mice using chemogenetic or optogenetic approaches induced depression-like behaviors including sociability deficiency, anxiety- and despair-related phenotypes (Fig. 4, Supplementary Fig. 8). Chemogenetic inactivation of this pathway also exacerbated depression-like behaviors in resilient mice (Fig. 5). Optogenetic activation of the Ent→V2M pathway in CSDS susceptible

Fig. 6 Activation of Ent→V2M projection terminals is antidepressant. a Schematic of ChR2 expression in the Ent→V2M projection terminals and functional test using fiber photometry in vivo. Ca^{2+} fluorescent dye (OGB-1, AM) was injected into superficial layers of the visual cortex. Fiber photometry (gray fiber) was used to image neural activity evoked by optogenetic activation (blue fiber) of axonal projections from Ent Va. **b** Example fluorescence trace evoked by presynaptic stimuli (blue bars) in the visual cortex under anesthesia. **c**, **d** Ca^{2+} related fluorescence increases evoked by laser stimulus (blue bar) (**c**) and spontaneous fluorescence increase under no laser stimulation (**d**). Red (in **c**) and blue lines (in **d**) indicate averaged activity trace. Gray lines, 60 laser stimuli-evoked events (**c**) and 29 spontaneous events (**d**). Dotted line, hypothetical fluorescence change during optogenetic stimulation. Laser power, 5 mW; duration, 100 ms. **e**, **f** Expression of ChR2-EYFP in Ent (**e**) and projection terminals in V2M (**f**). Scale bars, 500 μm (in **e**); 200 μm (in **f**). **g**, **h** Schematic of laser stimuli on the surface of the visual cortex (**g**) and laser stimulus profile (**h**). Laser was delivered in repeats with a 500 ms stimulus period followed with a 1 s interval. **i** Experimental timeline of viral injection, CSDS, fiber implantation and behavioral tests during optogenetic activation. **j**, **k** Activation of the Ent→V2M projection terminals promotes social interaction. The social index in CSDS mice was increased (**j**) while the avoidance index was decreased (**k**) during optogenetic activation. There was no difference between control and susceptible groups during optogenetic activation, indicating that activation of this pathway restored normal interaction in CSDS mice (**j**, **k**). **l** Control mice spent more time in the interaction zone than that in the corner zone during SIT. **m** Susceptible mice spent more time in the interaction zone than in the corner zone when the CD1 mouse was absent but this phenomenon was reversed when the CD1 mouse was present. Time in the interaction zone was increased while time spent in the corner zone was decreased during optogenetic activation in susceptible mice. $n = 6$ control mice and 8 susceptible mice. **n**–**q** Susceptible mice explored more in open arms of EPM (**n**, **o**) and in central area of OFT (**p**, **q**) as quantified by exploration duration (**n**, **p**) and number of entries (**o**, **q**) during optogenetic activation. There was no difference between control and susceptible groups during optogenetic activation, indicating that activation restored normal level of exploration in susceptible mice (**n**–**q**). $n = 6$ control mice and 10~11 susceptible mice. **r** Optogenetic activation decreased immobile time of susceptible mice in FST. $n = 6$ control mice and 9 susceptible mice. **s** Optogenetic activation decreased immobile time of susceptible mice in TST. $n = 6$ control mice and 9 susceptible mice. Statistics, *t*-test or Mann-Whitney U test for between-group comparison and one-way ANOVA followed by Sidak post hoc test for intragroup comparison. $^{***}P < 0.001$, $^{**}P < 0.01$, $^{*}P < 0.05$, n.s. Not significant. Data are shown as mean ± s.e.m.

animals rapidly alleviated the social deficiency, anxiety- and despair-like phenotypes, demonstrating the antidepressant effect of activating this pathway in mice (Fig. 6). The antidepressant effect of acute activation of the Ent→V2M pathway imply that elevated activity in the pathway has a therapeutic effect. As a shallow cortical circuit from deep brain area (Ent) to superficial cortical area (V2M, especially to superficial layer II/III), Ent→V2M pathway could be a great target for noninvasive stimulation therapy (such as rTMS and tDCS) of major depression. The antidepressant effect by specifically activating the Ent→V2M pathway in MDD patients requires confirmation.

Major depression has been viewed as a 'circuitopathy' [48]. Activity of the Ent→V2M pathway promotes the transition to anxiolytic- and antidepressant-like states (Fig. 7). The persistent neural activity of the pathway also correlates with continuous reward, and may need reciprocal excitation from many other brain areas [49], indicating the Ent→V2M pathway might be involved in a multi-regional network that regulates depression. There are several pathways, such as vHPC→mPFC [50, 51], Ent II→DG [20], mPFC→DRN (dorsal raphe nucleus) [52], and pBLA→vCA1 [53] that positively regulate anxiety- or (and) depression-like behaviors. Conversely, the neural activity of some brain regions and neural circuits mediates negative valence information and modulate stress related behaviors. For example, increasing activity of lateral habenula (LHb) neurons and LHb→RMTg (retromedial tegmental nucleus) circuit mediate depression-like behaviors [54–56]. The activity of posterior insular cortex (pIC)→central amygdala (CeA) pathway encodes aversive sensory information (i.e., pain, bitter taste and fear) and promotes anxiety-like behaviors [57]. The neural pathways from anterior basolateral amygdala (aBLA) to ventral hippocampal CA1 [53], from vHPC to NAc [58], and from BLA cholecystokinin glutamatergic neurons to NAc D2 neurons [35] mediate depression- or (and) anxiety-like behaviors. These findings imply that there may exist multi-regional networks (i.e., positive and negative networks) in the brain that positively or negatively modulate mental states and related behavioral phenotypes. Coordination of these two types of networks is required to maintain normal psychological states. Activation of the Ent→V2M pathway is both anxiolytic and antidepressant, and thus the pathway is part of a positive network.

Pulsed or continuous light illumination plays a pivotal role in modulation of mood and related psychiatric disorders through pathways from retina to specific subcortical areas [45–47]. However, the depression-like phenotypes in our study are not ameliorated by the leaked light illumination (Supplementary Fig. 11). Moreover, stressed animals with blinders to block normal visual stimulus maintain high level of social avoidance and anxiety-like behavioral phenotypes (Supplementary Fig. 11). Optogenetic activation of the Ent→V2M pathway under the blinder condition is still antidepressant (Supplementary Fig. 11). The Ent→V2M pathway does not consistently respond to consecutive LED light flashes (Supplementary Fig. 12). The activity of Ent→V2M pathway promotes anxiolytic- and antidepressant-like behaviors (Fig. 7), and this activity shows no change with normal visual stimulus diminished during red light illumination (which is blind to mice, Supplementary Fig. 12). These results suggest that the antidepressant effect of activating the Ent→V2M pathway does not depend on altered visual perception. Consistently, clinical studies report that TMS over secondary visual cortex (V2) of subjects elicits lower brightness of phosphenes than stimuli over primary visual cortex (V1) [59]. And 51 MDD patients that received rTMS over visual cortex, including V1 (27 cases) and a specific high order visual cortical area that responds more to fast neutral image viewing (24 cases), almost all have normal visual perception [11].

Visual cortex has been implicated in depression and the visual cortex of MDD patients has multiple abnormalities, including reduction of total cortical surface, reduction in neuron number and functional connectivity with frontoparietal networks, diminished response to emotional stimuli, and abnormal filtering of non-emotional stimuli [60–63]. Direct activation of visual cortex using rTMS (targeting the higher order visual cortex) rapidly alleviates depression symptoms [11] and fluoxetine treatment in MDD patients activates developmental-like neuronal plasticity in visual cortex [64], suggesting that visual cortex is one key area in regulation of depression. The primary visual cortex relays sensory information to higher order visual cortical areas (i.e., V2) and emotion-processing areas such as the hippocampus (via Ent), frontal cortical area (ACC), amygdala and striatum [65]. Visual cortex also receives feedback projections from areas including the hippocampus (via Ent Va) and ACC. These results imply that visual cortex functions as a key node in the network for modulation of mood and mood-related disorders such as depression and anxiety. How distinct neural circuits coordinate with each other to maintain normal psychological condition and modulate depression require further study.

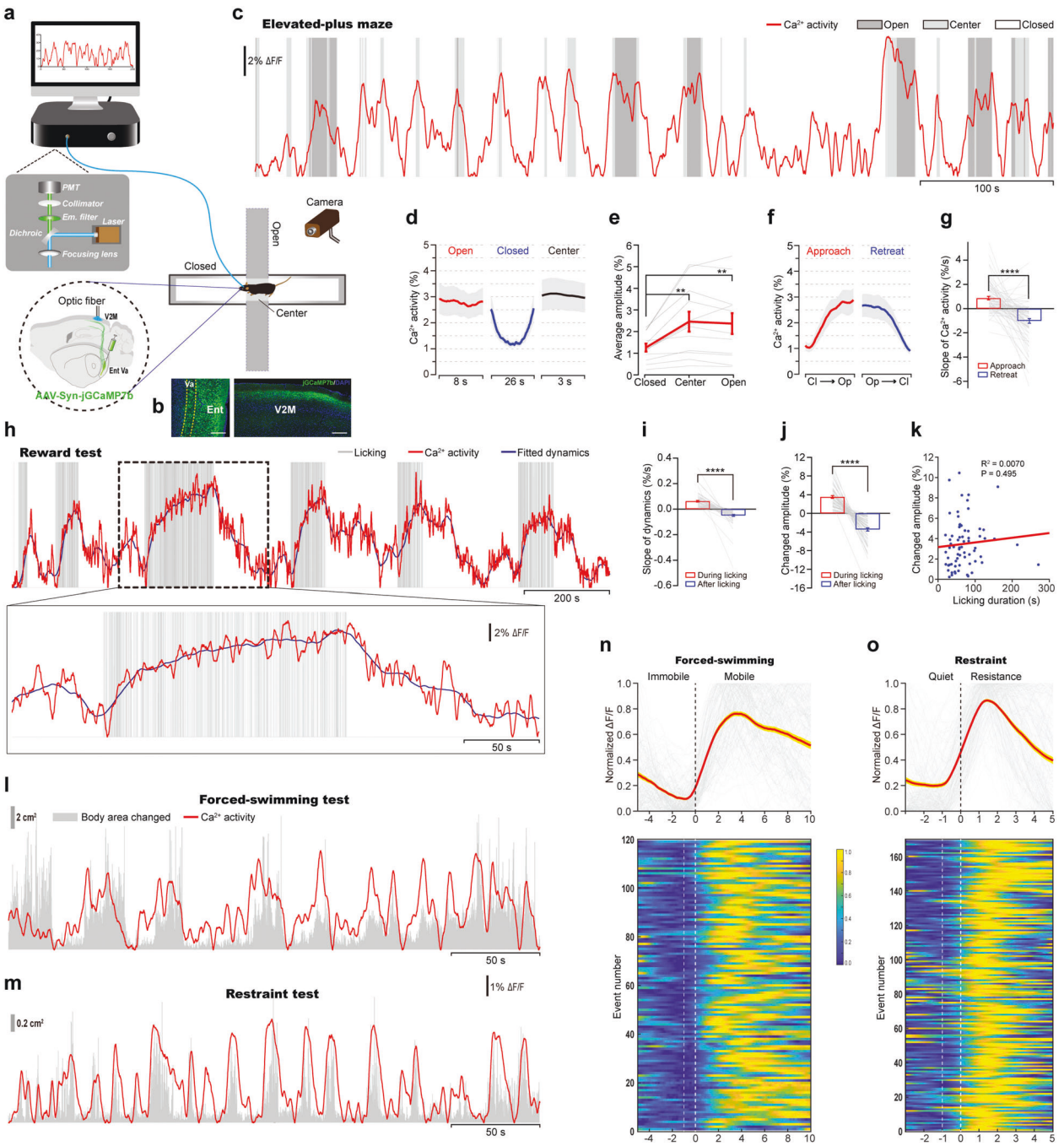

Fig. 7 Elevated neural activity of the Ent→V2M projection terminals promotes antidepression. a Schematic of fiber photometry during behavioral tests. A video camera was used to track the trajectory of mice. Genetically encoded calcium indicator jGCaMP7b was injected into Ent Va and an optical fiber implanted over V2M was used to monitor activity of the Ent→V2M projection terminals. The light path of fiber photometry is shown in the left middle figure. PMT, photomultiplier tube. **b** jGCaMP7b expression in Ent Va neurons (left) and their axonal projections in V2M (right). Scale bar, 200 μm. **c** Example neural dynamics of the Ent→V2M projection terminals in a mouse freely exploring an elevated-plus maze. Red, Ca^{2+} signal. Deep gray shadow indicates open arms. Light gray shadow indicates the center. The rest (white) indicates closed arms. **d** Ca^{2+} activity of the Ent→V2M projection terminals during exploration in the open arms, center and closed arms of EPM. Solid line, mean; gray shaded area, s.e.m.; $n = 12$ mice. **e** Mean amplitude of Ca^{2+} activity during exploration in the open arms and center is significantly larger than that in the closed arms. **f** Ca^{2+} activity increases when mice moved from closed to open arms and decreases when mice moved from open to closed arms. Red, closed arm to open arm (Cl → Op); blue, open arm to closed arm (Op → Cl). **g** Slope of Ca^{2+} activity change when mice transported between different arms (Cl → Op and Op→Cl). $n = 75$ events from 12 mice. **h** Example fluorescence trace of the Ent→V2M projection terminals during epochs of licking. Bottom, zoom in of the trace in the dashed box. Gray, licking events; blue, fitted dynamics. **i–k** The slope (**i**), amplitude of change (**j**) and correlation between change amplitude and duration (**k**) of the fitted dynamics during and after licking epochs. $n = 70$ events from 12 mice. **l, m** Example fluorescence trace of the Ent→V2M projection terminals during forced-swimming test (**l**) and restraint test (**m**). Gray shaded area indicates change of body area. **n, o** Normalized Ca^{2+} activity (to change amplitude during each event) aligned to movement start in FST (**n**) and restraint test (**o**). $n = 119$ events from 9 mice for FST, and $n = 169$ events from 5 mice for restraint test. Bottom, heatmap of individual events. Statistics, one-way ANOVA followed by Sidak post hoc test, paired t-test and Pearson correlation. $^{****}P < 0.0001$, $^{**}P < 0.01$. Data are shown as mean ± s.e.m.

REFERENCES

1. James SL, Abate D, Abate KH, Abay SM, Abbafati C, Abbasi N, et al. Global, regional, and national incidence, prevalence, and years lived with disability for 354 diseases and Injuries for 195 countries and territories, 1990-2017: A systematic analysis for the Global Burden of Disease Study 2017. Lancet. 2018;392:1789–858.
2. O'Reardon JP, Solvason HB, Janicak PG, Sampson S, Isenberg KE, Nahas Z, et al. Efficacy and safety of transcranial magnetic stimulation in the acute treatment of major depression: A multisite randomized controlled trial. Biol Psychiatry. 2007;62:1208–16.
3. Downar J, Daskalakis ZJ. New targets for rTMS in depression: A review of convergent evidence. Brain Stimulation. 2013;6:231–40.
4. Blumberger DM, Vila-Rodriguez F, Thorpe KE, Feffer K, Noda Y, Giacobbe P, et al. Effectiveness of theta burst versus high-frequency repetitive transcranial magnetic stimulation in patients with depression (THREE-D): A randomised non-inferiority trial. Lancet. 2018;391:1683–92.
5. Chase HW, Boudewyn MA, Carter CS, Phillips ML. Transcranial direct current stimulation: A roadmap for research, from mechanism of action to clinical implementation. Mol Psychiatry. 2020;25:397–407.
6. Stubbeman WF, Zarrabi B, Bastea S, Ragland V, Khairkhah R. Bilateral neuronavigated 20Hz theta burst TMS for treatment refractory depression: An open label study. Brain Stimulation. 2018;11:953–5.
7. Brunoni AR, Moffa AH, Sampaio-Junior B, Borrione L, Moreno ML, Fernandes RA, et al. Trial of electrical direct-current therapy versus escitalopram for depression. N. Engl J Med. 2017;376:2523–33.
8. Bakker N, Shahab S, Giacobbe P, Blumberger DM, Daskalakis ZJ, Kennedy SH, et al. RTMS of the dorsomedial prefrontal cortex for major depression: Safety, tolerability, effectiveness, and outcome predictors for 10 Hz versus intermittent theta-burst stimulation. Brain Stimulation. 2015;8:208–15.
9. Razza LB, Palumbo P, Moffa AH, Carvalho AF, Solmi M, Loo CK, et al. A systematic review and meta-analysis on the effects of transcranial direct current stimulation in depressive episodes. Depression anxiety. 2020;37:594–608.
10. Sampaio B, Tortella G, Borrione L, Moffa AH, Machado-Vieira R, Cretaz E, et al. Efficacy and safety of transcranial direct current stimulation as an add-on treatment for bipolar depression: A randomized clinical trial. JAMA Psychiatry. 2018;75:158–66.
11. Zhang Z, Zhang H, Xie CM, Zhang M, Shi Y, Song R, et al. Task-related functional magnetic resonance imaging-based neuronavigation for the treatment of depression by individualized repetitive transcranial magnetic stimulation of the visual cortex. Sci China Life Sci. 2020. 2020. https://doi.org/10.1007/s11427-020-1730-5.
12. Furtado CP, Maller JJ, Fitzgerald PB. A magnetic resonance imaging study of the entorhinal cortex in treatment-resistant depression. Psychiatry Res - Neuroimaging. 2008;163:133–42.
13. Kim Y, Perova Z, Mirrione MM, Pradhan K, Henn FA, Shea S, et al. Whole-brain mapping of neuronal activity in the learned helplessness model of depression. Front Neural Circuits. 2016;10:1–11.
14. Cheng W, Rolls ET, Qiu J, Liu W, Tang Y, Huang CC, et al. Medial reward and lateral non-reward orbitofrontal cortex circuits change in opposite directions in depression. Brain 2016;139:3296–309.
15. Gos T, Günther K, Bielau H, Dobrowolny H, Mawrin C, Trübner K, et al. Suicide and depression in the quantitative analysis of glutamic acid decarboxylase-Immunoreactive neuropil. J Affect Disord. 2009;113:45–55.
16. Uezato A, Meador-Woodruff JH, McCullumsmith RE. Vesicular glutamate transporter mRNA expression in the medial temporal lobe in major depressive disorder, bipolar disorder, and schizophrenia. Bipolar Disord. 2009;11:711–25.
17. Michel TM, Frangou S, Camara S, Thiemeyer D, Jecel J, Tatschner T, et al. Altered glial cell line-derived neurotrophic factor (GDNF) concentrations in the brain of patients with depressive disorder: A comparative post-mortem study. Eur Psychiatry. 2008;23:413–20.
18. Zhang C, Lueptow LM, Zhang HT, O'Donnell JM, Xu Y. The role of phosphodiesterase-2 in psychiatric and neurodegenerative disorders. Adv Neurobiol. 2017;17:307–347.
19. Chen X, Lan T, Wang Y, He Y, Wu Z, Tian Y, et al. Entorhinal cortex-based metabolic profiling of chronic restraint stress mice model of depression. Aging 2020;12:3042–52.
20. Yun S, Reynolds RP, Petrof I, White A, Rivera PD, Segev A, et al. Stimulation of entorhinal cortex-dentate gyrus circuitry is antidepressive. Nat Med. 2018;24:658–66.
21. Kobayashi K, Yoshinaga H, Ohtsuka Y. Memory enhancement and deep-brain stimulation of the entorhinal area. N Engl J Med. 2012;366:1945.
22. Stone SSD, Teixeira CM, de Vito LM, Zaslavsky K, Josselyn SA, Lozano AM, et al. Stimulation of entorhinal cortex promotes adult neurogenesis and facilitates spatial memory. J Neurosci. 2011;31:13469–84.
23. Kim CS, Chang PY, Johnston D. Enhancement of dorsal hippocampal activity by knockdown of hcn1 channels leads to anxiolytic- and antidepressant-like behaviors. Neuron 2012;75:503–16.
24. Tunc-Ozcan E, Peng CY, Zhu Y, Dunlop SR, Contractor A, Kessler JA. Activating newborn neurons suppresses depression and anxiety-like behaviors. Nat Commun. 2019;10:1–9.
25. Sürmeli G, Marcu DC, McClure C, Garden DLF, Pastoll H, Nolan MF. Molecularly defined circuitry reveals input-output segregation in deep layers of the medial entorhinal cortex. Neuron 2015;88:1040–53.
26. Kitamura T, Ogawa SK, Roy DS, Okuyama T, Morrissey MD, Smith LM, et al. Engrams and circuits crucial for systems consolidation of a memory. Science 2017;356:73–78.
27. Ohara S, Onodera M, Simonsen ØW, Yoshino R, Hioki H, Iijima T, et al. Intrinsic Projections of Layer Vb Neurons to Layers Va, III, and II in the Lateral and Medial Entorhinal Cortex of the Rat. Cell Rep. 2018;24:107–16.
28. Yue Y, Zong W, Li X, Li J, Zhang Y, Wu R, et al. Long-term, in toto live imaging of cardiomyocyte behaviour during mouse ventricle chamber formation at single-cell resolution. Nat Cell Biol. 2020;22:332–40.
29. Golden SA, Covington HE, Berton O, Russo SJ. A standardized protocol for repeated social defeat stress in mice. Nat Protoc. 2011;6:1183–91.
30. Lu J, Gong X, Yao X, Guang Y, Yang H, Ji R, et al. Prolonged chronic social defeat stress promotes less resilience and higher uniformity in depression-like behaviors in adult male mice. Biochemical Biophysical Res Commun. 2021;553:107–13.
31. Guo H, Huang ZL, Wang W, Zhang SX, Li J, Cheng K, et al. iTRAQ-based proteomics suggests Ephb6 as a potential regulator of the ERK pathway in the prefrontal cortex of chronic social defeat stress model mice. Proteom - Clin Appl. 2017;11:1–12.
32. He Y, Li W, Tian Y, Chen X, Cheng K, Xu K, et al. iTRAQ-based proteomics suggests LRP6, NPY and NPY2R perturbation in the hippocampus involved in CSDS may induce resilience and susceptibility. Life Sci. 2018;211:102–17.
33. Guo B, Chen J, Chen Q, Ren K, Feng D, Mao H, et al. Anterior cingulate cortex dysfunction underlies social deficits in Shank3 mutant mice. Nat Neurosci. 2019;22:1223–34.
34. Atasoy D, Nicholas Betley J, Su HH, Sternson SM. Deconstruction of a neural circuit for hunger. Nature 2012;488:172–7.
35. Shen CJ, Zheng D, Li KX, Yang JM, Pan HQ, Yu XD, et al. Cannabinoid CB1 receptors in the amygdalar cholecystokinin glutamatergic afferents to nucleus accumbens modulate depressive-like behavior. Nat Med. 2019;25:337–49.
36. Farrell MS, Roth BL. Pharmacosynthetics: Reimagining the pharmacogenetic approach. Brain Res. 2013;1511:6–20.
37. Sternson SM, Roth BL. Chemogenetic tools to interrogate brain functions. Annu Rev Neurosci. 2014;37:387–407.
38. Gunaydin LA, Grosenick L, Finkelstein JC, Kauvar IV, Fenno LE, Adhikari A, et al. Natural neural projection dynamics underlying social behavior. Cell 2014;157:1535–51.
39. Cui G, Jun SB, Jin X, Luo G, Pham MD, Lovinger DM, et al. Deep brain optical measurements of cell type-specific neural activity in behaving mice. Nat Protoc. 2014;9:1213–28.
40. Zhong W, Li Y, Feng Q, Luo M. Learning and stress shape the reward response patterns of serotonin neurons. J Neurosci. 2017;37:8863–75.
41. Renier N, Adams EL, Kirst C, Wu Z, Azevedo R, Kohl J, et al. Mapping of brain activity by automated volume analysis of immediate early genes. Cell 2016;165:1789–802.
42. Zhang Z, Yao X, Yin X, Ding Z, Huang T, Huo Y, et al. Multi-Scale Light-Sheet Fluorescence Microsc Fast Whole Brain Imaging. Front Neuroanat. 2021;15:732464.
43. Armbruster BN, Li X, Pausch MH, Herlitze S, Roth BL. Evolving the lock to fit the key to create a family of G protein-coupled receptors potently activated by an inert ligand. Proc Natl Acad Sci USA. 2007;104:5163–8.
44. Dana H, Sun Y, Mohar B, Hulse BK, Kerlin AM, Hasseman JP, et al. High-performance calcium sensors for imaging activity in neuronal populations and microcompartments. Nat Methods. 2019;16:649–57.
45. Huang L, Xi Y, Peng Y, Yang Y, Huang X, Fu Y, et al. A visual circuit related to habenula underlies the antidepressive effects of light therapy. Neuron 2019;102:128–42.e8.
46. An K, Zhao H, Miao Y, Xu Q, Li Y, Ma Y, et al. A circadian rhythm-gated subcortical pathway for nighttime-light-induced depressive-like behaviors in mice. Nat Neurosci. 2020. June 1, 2020. https://doi.org/10.1038/s41593-020-0640-8.
47. Zhou Z, Liu X, Chen S, Zhang Z, Liu Y, Montardy Q, et al. A VTA GABAergic neural circuit mediates visually evoked innate defensive responses. Neuron 2019;103:473–88.e6.
48. Lozano AM, Lipsman N. Probing and regulating dysfunctional circuits using deep brain stimulation. Neuron 2013;77:406–24.
49. Guo ZV, Inagaki HK, Daie K, Druckmann S, Gerfen CR, Svoboda K. Maintenance of persistent activity in a frontal thalamocortical loop. Nature 2017;545:181–6.
50. Carreno FR, Donegan JJ, Boley AM, Shah A, DeGuzman M, Frazer A, et al. Activation of a ventral hippocampus-medial prefrontal cortex pathway is both necessary and sufficient for an antidepressant response to ketamine. Mol Psychiatry. 2016;21:1298–308.
51. Padilla-Coreano N, Bolkan SS, Pierce GM, Blackman DR, Hardin WD, Garcia-Garcia AL, et al. Direct ventral hippocampal-prefrontal input is required for anxiety-related neural activity and behavior. Neuron 2016;89:857–66.

52. Warden MR, Selimbeyoglu A, Mirzabekov JJ, Lo M, Thompson KR, Kim SY, et al. A prefrontal cortex-brainstem neuronal projection that controls response to behavioural challenge. Nature 2012;492:428–32.
53. Pi G, Gao D, Wu D, Wang Y, Lei H, Zeng W, et al. Posterior basolateral amygdala to ventral hippocampal CA1 drives approach behaviour to exert an anxiolytic effect. Nat Commun. 2020;11:1–15.
54. Yang Y, Cui Y, Sang K, Dong Y, Ni Z, Ma S, et al. Ketamine blocks bursting in the lateral habenula to rapidly relieve depression. Nature 2018;554:317–22.
55. Cui Y, Yang Y, Ni Z, Dong Y, Cai G, Foncelle A, et al. Astroglial Kir4.1 in the lateral habenula drives neuronal bursts in depression. Nature 2018;554:323–7.
56. Proulx CD, Aronson S, Milivojevic D, Molina C, Loi A, Monk B, et al. A neural pathway controlling motivation to exert effort. Proc Natl Acad Sci USA. 2018;115:5792–7.
57. Gehrlach DA, Dolensek N, Klein AS, Roy Chowdhury R, Matthys A, Junghänel M, et al. Aversive state processing in the posterior insular cortex. Nat Neurosci. 2019;22:1424–37.
58. Bagot RC, Parise EM, Peña CJ, Zhang HX, Maze I, Chaudhury D, et al. Ventral hippocampal afferents to the nucleus accumbens regulate susceptibility to depression. Nat Commun. 2015;6:7062.
59. Salminen-Vaparanta N, Vanni S, Noreika V, Valiulis V, Móró L, Revonsuo A. Subjective characteristics of TMS-induced phosphenes originating in human V1 and V2. Cereb Cortex. 2014;24:2751–60.
60. Schmaal L, Hibar DP, Sämann PG, Hall GB, Baune BT, Jahanshad N, et al. Cortical abnormalities in adults and adolescents with major depression based on brain scans from 20 cohorts worldwide in the ENIGMA major depressive disorder working group. Mol Psychiatry. 2017;22:900–9.
61. Maciag D, Hughes J, O'Dwyer G, Pride Y, Stockmeier CA, Sanacora G, et al. Reduced density of Calbindin Immunoreactive GABAergic neurons in the occipital cortex in major depression: Relevance to neuroimaging studies. Biol Psychiatry. 2010;67:465–70.
62. Desseilles M, Balteau E, Sterpenich V, Thien TDV, Darsaud A, Vandewalle G, et al. Abnormal neural filtering of irrelevant visual information in depression. J Neurosci. 2009;29:1395–403.
63. Furey ML, Drevets WC, Hoffman EM, Frankel E, Speer AM, Zarate CA. Potential of pretreatment neural activity in the visual cortex during emotional processing to predict treatment response to scopolamine in major depressive disorder. JAMA Psychiatry. 2013;70:280–90.
64. Castrén E, Rantamäki T. The role of BDNF and its receptors in depression and antidepressant drug action: Reactivation of developmental plasticity. Developmental Neurobiol. 2010;70:289–97.
65. Han Y, Kebschull JM, Campbell RAA, Cowan D, Imhof F, Zador AM, et al. The logic of single-cell projections from visual cortex. Nature 2018;556:51–6.

ACKNOWLEDGEMENTS

We thank Hailan Hu, Cheng Zhan and Ji Hu for comments on the manuscript. We also thank Pengfei Wei, Yu Wang, Yan Huo, Tianyi Huang, Fan Di, Hongjiang Yang, Yuexin Yang and Xiao Yao for generous assistance in the experiments of animal breeding, electrophysiological recording and morphology; the Cell Biology Facility, Center of Biomedical Analysis at Tsinghua University for imaging of brain sections; the Animal Core Facility at Tsinghua University for maintaining the mouse lines. This work was supported by the National Natural Science Foundation of China (32021002) to ZVG and the National Key R&D Program of China (2017YFA0505700) to PX.

AUTHOR CONTRIBUTIONS

JL, ZVG, and PX conceived the project. JL performed the experiments with inputs from ZZZ (Light-sheet fluorescence imaging), XXY (Reward licking setup and code programing), YJT (Fiber photometry), YG, XG, YH, WZ, HYW, KC, YW (CSDS modeling and behavior tests) and XWC (Ent→Visual cortical projection tracing). JL analyzed the data with inputs from RNJ and HC (code programing). JL and ZVG wrote the manuscript with comments from other authors.

COMPETING INTERESTS

The authors declare no competing interests.

ADDITIONAL INFORMATION

Supplementary information The online version contains supplementary material available at https://doi.org/10.1038/s41380-022-01540-8.

Correspondence and requests for materials should be addressed to Peng Xie or Zengcai V. Guo.

Reprints and permission information is available at http://www.nature.com/reprints

Publisher's note Springer Nature remains neutral with regard to jurisdictional claims in published maps and institutional affiliations.